ROYAL SOCIETY
OF CHEMISTRY

PAPER

Correlation between structural and electronic order–disorder effects and optical properties in ZnO nanocrystals

F. A. La Porta,*[ab] J. Andrés,[b] M. V. G. Vismara,[c] C. F. O. Graeff,[c] J. R. Sambrano,[d] M. S. Li,[e] J. A. Varela[a] and E. Longo[a]

The correlation between structural and electronic order–disorder effects in understanding the optical properties of flower-like ZnO nanocrystals synthesized by the microwave-assisted hydrothermal method at low temperatures and short times is discussed. Theoretical simulations were performed at the density functional theory level to gain a better understanding of the experimental data from X-ray diffraction (XRD), field emission scanning electron microscopy (FE-SEM), electron paramagnetic resonance (EPR), ultraviolet-visible diffuse reflectance (UV-vis) spectroscopy and photoluminescence (PL) measurement studies at different temperatures. The decrease in band gap values is due to the presence of intermediate states above the conduction band. These discrete levels are formed by structural and electronic disorder of tetrahedral [ZnO$_4$] clusters which enhance the electron–hole pair.

1. Introduction

Due to the unique properties of ZnO as well as the simplicity of fabrication, a wealth of studies have been published on the synthesis, structural characterization and chemical/physical properties of ZnO nanostructures[1,2] with unprecedented capabilities in emerging technologies ranging from optoelectronics to the biomedical field.[3–6]

Although defined ZnO nanostructures with different morphologies have been reported using a variety of procedures,[7–12,29] existing methods require either harsh conditions, complex procedures or long reaction times. In addition, although it is well-known that the presence of lattice defects plays a key role in the physical and chemical properties of ZnO nanostructures,[10,11] many questions still remain due to the lack of conclusive evidence for defects responsible for luminescence properties.[13]

In recent years, microwave-assisted chemistry is emerging as a powerful and innovative tool in all areas of synthetic chemistry due to its advantages over other synthetic methods,[14–16] such as shortened reaction times, cost-effectiveness, and cleaner reactions compared to conventional routes.[16,17] In particular, Kappe *et al.*[18] reported a critical assessment of the specific role of microwave irradiation in the synthesis of ZnO micro- and nanostructured materials. This synthetic procedure provides an economically viable route for applications but also opens a new avenue to study the structural kinetics and chemistry of semiconductors and nanocrystals.[16,17] The microwave-assisted hydrothermal (MAH) method has been employed previously by our group to produce interesting morphologies for a wide range of metal oxides,[18–21] including ZnO.[22,23]

Disorder effects in the preparation of nanocrystalline semiconductor materials open a new field of study in nanotechnology dedicated to the understanding, interpretation and rationalization of physical properties and their origins at the atomic level.[11,24–26] However, the origin and the influence of disorder in nanoparticles are still under debate. The term "disorder" can be misleading because it is used to encompass a very large number of different phenomena.[27] In this context, our objective is focused primarily on two specific aspects: structural and electronic order–disorder effects that favor the self-trapping of electrons and the charge transfer processes on ZnO nanocrystals synthesized by the MAH method in short times. The samples were characterized by X-ray diffraction (XRD), field emission scanning electron microscopy (FE-SEM), electron paramagnetic resonance (EPR), ultraviolet visible (UV-vis) spectroscopy and photoluminescence (PL) measurements. The origin of intense PL bands was investigated by first-principles quantum mechanical calculations based on the density functional theory (DFT) and discussed in light of the cluster concept.

[a]*Instituto de Química, UNESP, P. O. Box 355, 14801-970, Araraquara, SP, Brazil. E-mail: felipe_laporta@yahoo.com.br; Fax: +55 163301 9691; Tel: +55 163301 9892*

[b]*Department of Analytical and Physical Chemistry, Univ Jaume I, Castelló de la Plana, 12071, Spain*

[c]*Departamento de Física-FC, UNESP, 17033-360 Bauru, Brazil*

[d]*Laboratório de Simulação Molecular, UNESP, P. O. Box 473, 17033-360, Bauru, SP, Brazil*

[e]*Departamento de Física, USP, P. O. Box 369, 13560-970 São Carlos, São Paulo, Brazil*

2. Methodology

2.1 Materials and synthesis

ZnO nanocrystals were synthesized by the MAH method using 1.5 mL of ammonium hydroxide (NH_4OH) (30% in NH_3, Synth) together with 7.34 mmol of zinc chloride which were dissolved in 40 mL of deionized water. In the sequence, the precursor aqueous solution was transferred into a Teflon autoclave which was properly sealed and placed inside a domestic microwave-solvothermal system (2.45 GHz, maximum power of 800 W) at 363 K for 10–120 min. The precipitated white powder was rinsed with deionized water and ethanol several times in sequence and extracted by centrifugation, followed by 343 K drying in air for 24 hours.

2.2 Characterization

The nanocrystals obtained were structurally characterized by XRD using a Rigaku-DMax/2500 PC with Cu K_α radiation (λ = 1.5406 Å) in the 2θ range from 10 to 75° at 0.02° min^{-1}. Morphologies of ZnO nanocrystals were observed by field emission scanning electron microscopy (FE-SEM) images using a FEG-VP JEOL. EPR measurements were conducted using a Magnetech MS300 spectrometer working in the X-band. Measurements were made at low temperature using a LN2 flow cryostat. Typically the temperature was maintained accurately at 1 K. The g-factor was calibrated using 2,2-diphenyl-1-picrylhydrazine (DPPH) and the number of spins was determined using an a-Si sample with a known number of spins. Samples were irradiated with a 1 mW UV-LED with emission at 370 nm for a minimum of at least 1 hour before conducting experiments. The effective g-factor is calculated using the equation:[28]

$$g_{eff} = \frac{h\nu}{|\mu_B| \cdot H_0}$$

1where h, ν, μ_B and H_0 are the Planck constant, frequency of the applied microwave field, Bohr magnetron and applied magnetic field, respectively.

Optical properties were analyzed by means of UV-vis reflectance spectra and PL measurements. The UV-vis diffuse reflectance spectra were recorded using a Cary 5G spectrophotometer (Varian, USA). PL spectra were collected with a Thermal Jarrel-Ash Monospec monochromator and a Hamamatsu R446 Photomultiplier. The 350.7 nm (3.54 eV) exciting wavelength of a krypton ion laser (Coherent Innova) was used with a measured power of 13 mW on the sample. During all measurements, the samples were in an inert atmosphere of helium gas, and thus there are no surface adsorbates.

2.3 Computational details

The model we have adopted is based on periodic boundary conditions and the calculations were performed at the DFT level with Becke's three-parameter hybrid nonlocal exchange functional[30] combined with the Lee–Yang–Parr gradient-corrected correlation functional[31] of approximation (B3LYP), as implemented in the CRYSTAL09 computer code.[32] The atomic centers have been described by all electron pob-TZVP basis sets for Zn and O atoms.[33] The level of calculation accuracy for the Coulomb and exchange series was controlled by five thresholds set to 10^{-8}, 10^{-8}, 10^{-8}, 10^{-8}, and 10^{-18}.[32] The shrinking (Monkhorst–Pack)[34] factor was set to 6, which corresponds to 80 independent k-points in the irreducible part of the Brillouin zone integration. This computational procedure has been employed previously on similar systems with success.[35–37]

In the present work, we focus on the effect of changes in the local structure and disorder on ZnO crystalline materials obtained by the MAH method. To better describe cluster distortion due to structural effects on the ZnO crystal, average distances of O and Zn atoms to the center of the cluster have been computed. The order can be related to an ideal $[ZnO_4]^\times$ cluster or $[ZnO_4]'$ while disorder can be related to a defective $[ZnO_4]'$ or $[ZnO_3 \cdot V_O^z]$ (see below). Based on the experimental results presented in this research, four periodic models were built from these optimized parameters to represent the ordered model ($[ZnO_3]^\times$–O–$[ZnO_3]^\times$) and disordered model ($[ZnO_4]^\times/[ZnO_3V_O^z]$) which are associated with oxygen vacancies, where $V_O^z = V_O^\times$, $V_O^\cdot$ or $V_O^{\cdot\cdot}$ as well as dislocating the Zn atom, 0.005, 0.1 and 0.2 Å, in the z-direction, respectively. These models can be useful to represent different degrees of order–disorder in the material and structural defects resulting from Zn displacements. Density of states (DOS), band gap, band structure, charge density and theoretical frequency modes have been performed and compared between the four models. The XcrysDen program[38] was used for band structure drawing design.

3. Results and discussion

Long-range structural order was determined by XRD patterns which elucidate that ZnO nanocrystals have a hexagonal wurtzite-analogous ($P6_3mc$) crystal structure (a = 3.24 Å and c = 5.21 Å) with high crystallinity and purity according to JCPDS card 36-1451 (see Fig. 1(a)). No characteristic impurity peaks were observed. UV-vis diffuse reflectance was used to determine the band gap of these materials and resulting spectra are shown in Fig. 1(b). The exponential optical absorption edge and the optical band gap energy are controlled by the degree of structural and electronic disorders in the ZnO lattice and thus allow tuning of their optical properties by band gap engineering.[39] For our samples, the band gap is direct with a value of ~3.2 eV which is in good agreement with values reported in the literature, 3.37 eV.[1,2,22,23]

The FE-SEM images of the ZnO nanocrystals prepared under MAH conditions are shown in Fig. 2. All the crystalline agglomerates of ZnO nanocrystals exhibit nanoflower shapes and correspond to a polydisperse sample. It can be seen that the nanostructures assembled by rod-like ZnO gathered gradually to form nanoflower-shaped ZnO with about ~76 nm in diameter and ~705 nm lengths. The size of the flower-like ZnO petals became more uniform with increasing reaction time in the MAH process. The MAH method results in micro- or nanocrystals with high purity and crystallinities at lower temperatures than conventional heating methods.[15–19] An elemental analysis reveals that the products contain only Zn and O atoms

This journal is © The Royal Society of Chemistry 2014

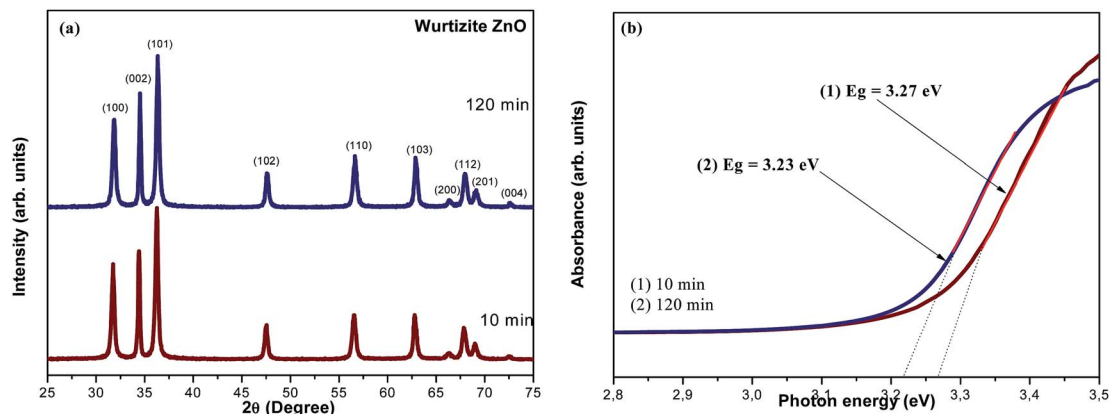*J. Mater. Chem. C*, 2014, **2**, 10164–10174 | **10165**

Fig. 1 (a) XRD patterns and (b) UV-vis spectra of ZnO nanocrystals processed by the MAH method.

(see Fig. 2(c)). These results verify that the material surfaces are similar and the chloride ions were removed during the washing process, in accordance with XRD patterns. However, poly-condensation takes place in solution, which can be controlled by adjusting the experimental variables, such as reaction time, temperature, pH, concentration, and precursors.[40,41] The use or not of surfactants can be used to control the growth of nano-particles to the desired size and shape by the MAH synthesis. Generally the synthesis proceeds *via* a nucleation–dissolution–recrystallization mechanism which is considered to be highly sensitive to relative rates of amorphous solid particle dissolution and nucleation of the crystalline phase.[40,41]

In particular, the nucleation and crystal growth stages of ZnO provoked by the MAH process can be separated very clearly. The presence of OH^- ions plays a key role in the growth mechanism of ZnO nanoflowers and their degree of crystal-linity, since these ions act in the process of formation of the $[Zn(OH)_4]^{2-}$ complex in aqueous solution, and which can be considered the basic units for the growth of ZnO nano-structures.[40,42–45] Our results suggest that the self-assembly process is responsible for producing flower-like ZnO micro-crystals from the aggregation of structures formed by several ZnO nanorods hierarchically ordered. Basically, the aggregation of ZnO nanorods occurs at the edge of the top face and the crystal growth process involves several stages during processing

in MAH. A detailed study of the growth process of the flower-like ZnO crystal is not part of the scope of this work and it will be the target for future studies.

EPR spectroscopy is one of the most sensitive and interesting analytical techniques for investigating, quantification and understanding of the microscopic nature of defects in inorganic solids.[46] More recently, Kaftelen *et al.*[47] have discussed in detail the spin state of the vacancies/defect centers for the ZnO nanomaterial by EPR results.

Fig. 3 illustrates EPR spectra of ZnO nanocrystals recorded at 198 K for both in the dark and under Ultraviolet Light-Emission Diode (UV-LED) illumination. Only one EPR line is observed with a *g* of ~1.96 which was the predominant paramagnetic defect observed in the two samples studied here synthesized by MAH for 10 and 120 min. In this case, for ZnO nanocrystals an EPR line with *g* ~1.96 is usually observed and the origin of this signal is still not fully established.[46–50] According to the litera-ture, this EPR signal can be associated with possible defects that are induced in the ZnO lattice, as zinc vacancies (V_{Zn}), oxygen on interstitial sites (O_i), mobile electrons either in the conduction band and/or shallow donor states and oxygen vacancies (V_O^z).[46–50] However the latter is the defects most commonly accepted for this EPR signal and are assigned to singly ionized oxygen vacancy defects (V_O^{+1}). This is evidenced by UV-light
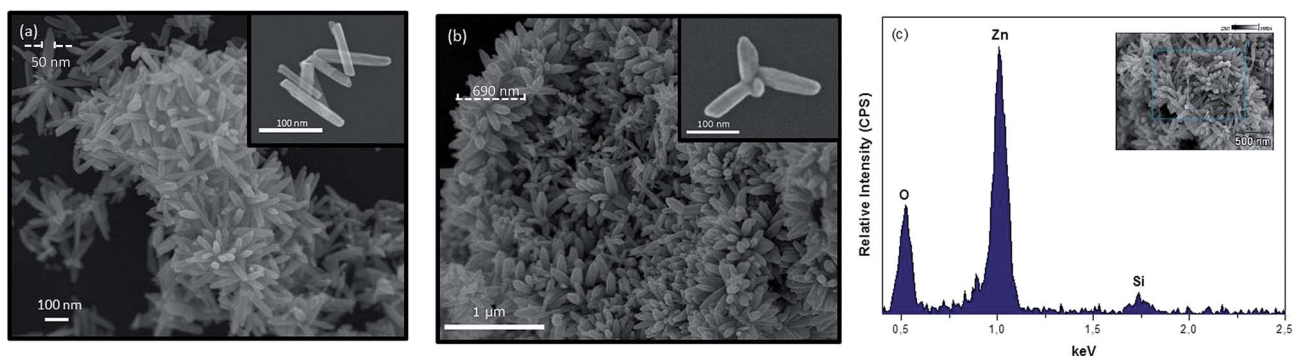

Fig. 2 FE-SEM images of ZnO samples: (a) 10 min and (b) 120 min and (c) EDS patterns.
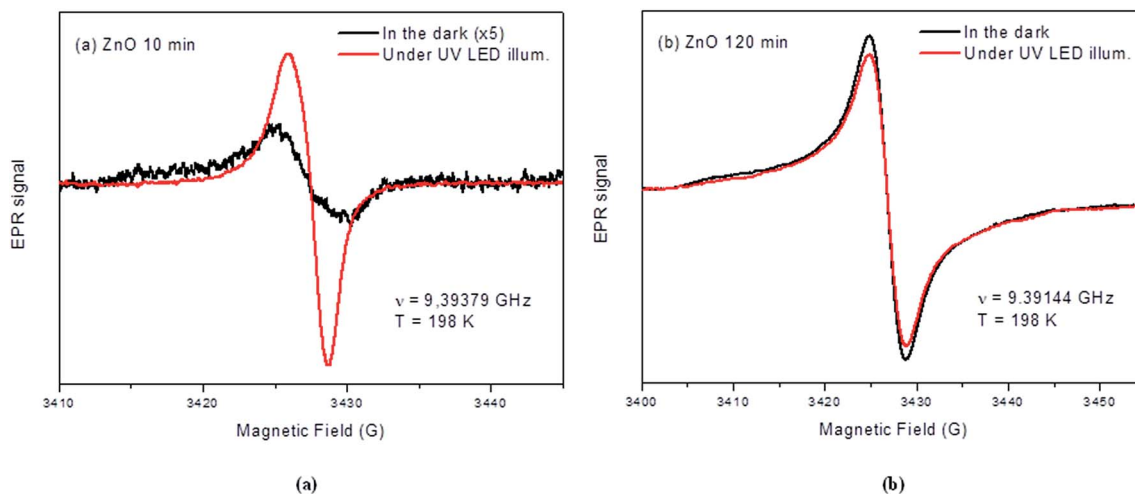
Fig. 3 EPR spectra of ZnO nanocrystals at 198 K in the dark and with LED–UV illumination. (a) 10 min and (b) 120 min.

irradiation that produces an increase in the EPR signal and is related to oxygen vacancy concentrations.[47–50]

Some reviews also showed beyond the EPR signal with g ∼1.96, and another signal at g ∼2.00 that is related to surface defects generated during the milling process. These surface defects are also still controversial and have also been assigned to a singly ionized Zn vacancy or to an unpaired electron trapped in an oxygen vacancy site.[47,49] However these paramagnetic surface defects were not observed in our samples.

In this context, we are assuming that the EPR signal is assigned to singly ionized oxygen vacancies (V_O^{+1}). Considerable efforts have been made to understand native defects in ZnO by theoretical calculations and experiments, since electronic properties are strongly coupled with the local structure and disorder in crystalline materials.[51–55] However, our focus in this study will be on understanding the charge state of the oxygen vacancy. It has been shown that oxygen vacancies contribute strongly to optical absorption in the visible spectral and are the origin of the red-shift in the PL emission.[51–55] In these previous studies, it has been discussed that the formation energies of intrinsic defects in ZnO, in particular, oxygen vacancies significantly vary, on the other hand, V_O^{+1} donor levels and V_O^{+2} energy levels are located in the energy band gap.

The UV-LED illumination on the intensity of EPR ZnO samples reveals a clear distinction between the different samples. An analysis of Fig. 3(a) reveals that the UV-LED illumination is followed by a sharp increase in the EPR absorption line. The spin density changes from 4×10^{14} spins per g in the dark to 4×10^{15} spins per g. One simple explanation is that under UV-LED illumination, the V_O^{2+} centers can trap the photoactivated electron and change it to V_O^{1+} which is paramagnetic. The line width changes from 3.0 G in the dark to 1.8 G under UV-LED conditions. However, an opposite effect was detected for ZnO nanocrystals synthesized for 120 min (see Fig. 3(b)); *i.e.*, UV-LED illumination has a very small effect with respect to the signal obtained in the dark, and in both cases, the spin density is orders of magnitude higher at 4×10^{16} spins per

g when compared to nanocrystals synthesized for 10 min. The significant difference between the EPR signal intensities under the influence of UV-LED illumination shown in Fig. 3 reveals that the photoinduced electrons were partially trapped at Zn cations and suggests that other electrons remain in the conduction band. By analyzing the results depicted in Fig. 3, we can observe that the EPR signal intensity increases under UV-LED illumination, and this behavior can be associated with structural and electronic order–disorder effects of both Zn or O atoms. These values are similar to those previously reported in the literature,[47–50] and a review of the subject has been reported by Hunger and Weitkamp.[56] To understand, the origins of the EPR signal could be assigned to the holes trapped on oxygen atoms, in particular, oxygen vacancies at the particle surface or bulk. Based on our EPR results, we can observe V_O^{+1} which was discussed previously, and also showed a mixture of V_O^0 and V_O^{+2} for these materials prepared by a microwave-assisted hydrothermal method. It is important to mention that the oxygen vacancies behave both as shallow and deep trap states in the crystalline lattice and play an important role in determining the physical properties of the lattice.

To further characterize the optical nature of ZnO nanocrystals, temperature-dependent PL spectra were recorded (see Fig. 4). For PL measurements, the 350.1 nm line of a krypton ion laser was used as the excitation source with a power of 13 mW. The emission spectral profile strongly depends on the excitation wavelength, since the use of different wavelengths promotes the excitation of electrons localized at different energy levels within the band gap. Fig. 4 shows temperature-dependent PL spectra of ZnO nanocrystals and a broad band covering visible electromagnetic spectra in the range of 400 to 800 nm from 290 K (red) to 6 K (light blue). A PL profile analysis reveals a common feature which is a soft peak in the UV region (439 nm) related to shallow trap emissions while a pronounced maximum is found in the orange region (602 and 610 nm for 10 min and 120 min, respectively) which is related to broad deep level defect emissions due to their presence within the band gap (see Fig. 4),

which were confirmed and characterized by UV-vis and EPR measurements (see Fig. 1(b) and 3, respectively), and the position and/or intensity of the maximum depends on the degree of structural order–disorder in the nanostructures, which are strongly influenced by the synthesis conditions.[57–60] Furthermore, it is well-known that the self-absorption of UV emission can excite defect states of electrons localized at different energy levels within the band gap in the ZnO nanocrystals resulting in a broad deep band.[60–63] The UV peak is due to the exciton-recombination process while the visible emission centered at about ~600 nm ranging from 480 to 800 nm is associated with oxygen vacancies due to the formation of deep levels in the band gap; this observation is also consistent with results reported by other groups.[7] In particular, Willander et al.[61] have reported a comprehensive review on the subject.

There is a common perception that the predominant structural and electronic disorders in ZnO are oxygen vacancies, which are responsible for n- and p-type properties under reducing and oxidizing conditions, respectively. From an electronic perspective, disorder is characterized by energy states above the valence band (VB) and below the conduction band (CB) which decreases the band gap. Bulk and surface defects may be possible trap sites and electron–hole recombination frequently occurs at these trap sites. The emission band profile is typical of a multiphonon process, where relaxation occurs by several paths which involve the participation of numerous states within the band gap of the material.[19,22,23] Furthermore, doping of the ZnO nanocrystals with different elements enables an adjustment of their optical properties in a wide-range of the electromagnetic spectrum.[64–66]

In this study, we present the general details about the description of the temperature dependence of the PL emission from ZnO nanocrystals, and the results suggest that the PL behavior is consistent with the phonon-assisted recombination which is in good agreement with other studies.[67,68] In particular, Van Vugt et al.[69] have reported a strong exciton–photon coupling in ZnO nanowires at room temperature. The phonon-assisted recombination determines the temperature-dependence of the PL signal intensity which decreases with an increase in temperature due to phonon-assisted transition effects in the ZnO crystal.

Furthermore, the intensity of the PL signal provides information on the quality of surfaces and interfaces of ZnO nanocrystals prepared by a MAH method. This intensity is likely associated with the structure organization level and the charge transfer occurring between oxygen and zinc ions. The relative PL intensity decreases by about 50% for a sample synthesized at longer times with the MAH system, which could be consistent with a decrease of disorder ZnO in the lattice. These results are in good agreement with the EPR measurements shown in Fig. 3. The PL intensity gives a measure of the relative rates of radiative and non-radiative recombination and is influenced by the temperature.

It has been reported that[70] energy relaxation in semiconductors is dominated by non-radiative processes at room temperature. At low temperatures, it has been reported that PL emissions are closely related to the high mobility of carriers under these conditions[71] and all energy relaxation events are radiative,[68] providing an increase in PL emission intensity because phonon-assisted transitions in ZnO nanocrystals are practically eliminated at cryogenic temperatures.[68] Similar results have been reported in the literature for ZnO nanocrystals[67,68] and other compounds.[71] The PL intensity improvement of the UV emission peak over the vacancy-related deep level emission peak occurs because of the better crystalline nature of the sample with a 10 to 120 min reaction time (see Fig. 4). The PL intensity improvement of the UV emission peak over the vacancy-related deep level emission peak is associated with the increase in crystallinity of these nanostructures for the samples synthesized by the MAH process. These results show a possible reduction in the concentration of defects in the sample prepared with the largest processing time under MAH conditions.

Several studies have been published regarding the origin of this orange emission band. The PL behavior involves the presence of impurities or structural defects in the crystal lattice distortions. These imperfections involve the short, medium and long distances that can generate optical properties in the ZnO range across the visible spectrum, leading to new applications.
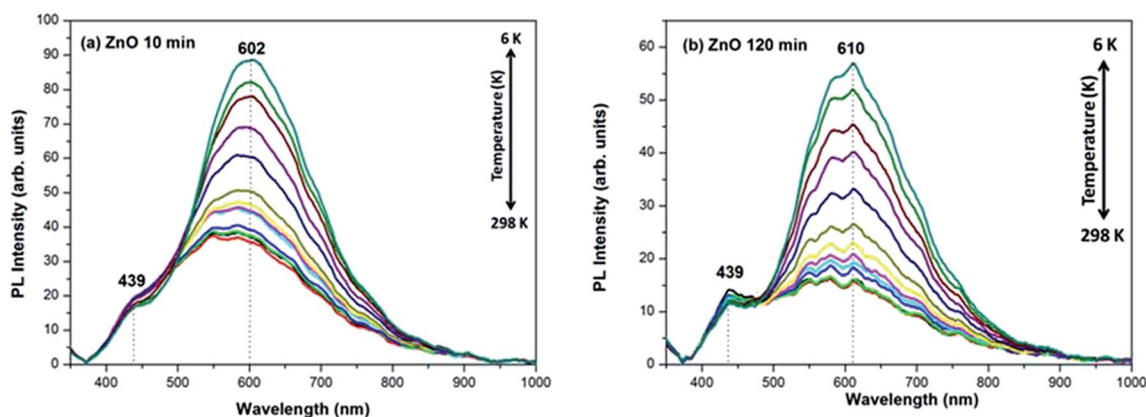

Fig. 4 A ZnO nanocrystal PL spectrum at different temperatures. (a) 10 min and (b) 120 min.

10168 | J. Mater. Chem. C, 2014, 2, 10164–10174

This journal is © The Royal Society of Chemistry 2014

Therefore characterization depends on the nature and structure of the imperfection and the electronic states of the solid.[59–63,67,68] In particular, all the defects discussed above play a key role in streamlining the physical and chemical properties of semiconductor materials directly associated with the structural and electronic order–disorder effects which can exist in ZnO nanocrystals with different charged states or in a neutral state typically represented by V_O^{2+}, V_O^{1+} or V_O^0,[60–63,72,73] which are generated in the rapid crystallization of such materials during the MAH process, and have been reported in this study. In this case, experimental results presented in Fig. 4 are in accord with the mechanism proposed by Bauer *et al.*[72] in explaining the green PL behaviour of ZnO, and show that the shift in PL emission can be due a fast recombination between electron–hole pairs in ZnO nanocrystals, and reveal that this disordered structure promotes polarization in the crystal structure, which corresponds to a positively charged oxygen vacancy and could be mainly responsible for PL behavior. The results indicate the relationship between the broad PL band and the degree of order–disorder in ZnO nanocrystals and are in agreement with other studies.[22,23,60–63,67,68]

A few years ago, we proposed a cluster model to explain complex metal oxide PL emissions of perovskite and scheelite-based materials.[73–76] In this model, the clusters are used as basic units of the materials to explain the structural and electronic order–disorder effects as well as their physical properties. In this study, we apply the cluster model to ZnO as a representative example of a non-centrosymmetric oxide where a $[ZnO_4]$ cluster with a 4-fold tetrahedral coordination acts as the constituent basic unit. The theoretical results reported, as it will be shown here, were performed on the ground state electronic structure and the related properties of order–disorder local effects on the bulk ZnO materials. Our study aims at providing an alternative picture into the electronic structure properties of ZnO nanocrystals, in terms of order–disorder effects on the chemical bonding of $[ZnO_4]$ tetrahedral clusters, and targeting a better understanding of the experimental data because, in general, the physical characteristics and the chemical behavior of nanocrystalline semiconductor materials are strongly influenced not only by size-induced effects such as quantum confinement and surface properties, but also by the local structure and disorder in crystalline materials such as statistical distributions in chemical bonding or defect densities that are increasingly recognized as the key in understanding the properties of many functional materials.[11,24–26,77–79]

The optimized wurtzite-type structure belongs to the hexagonal space group $P6_3mc$ with the lattice parameters: $a = 3.284$, $c = 5.214$ Å and $u = 0.380$ and contains two formula units of
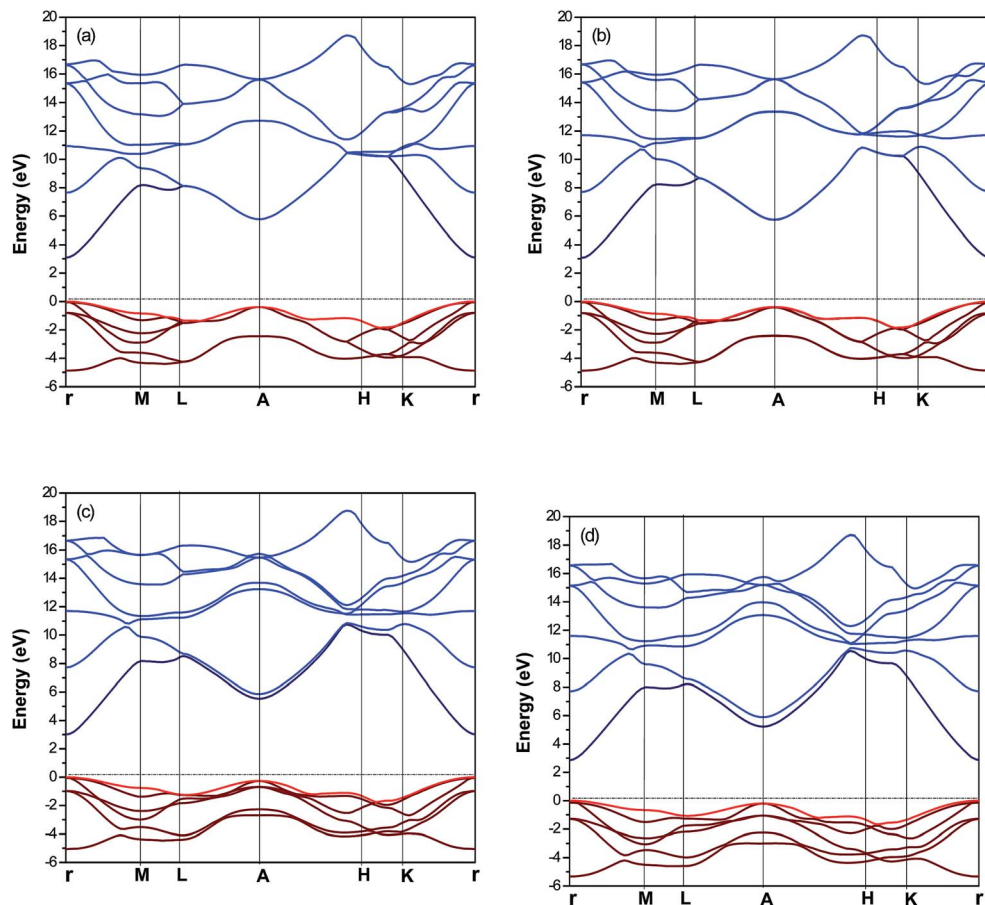

Fig. 5 Band structures for the ordered (a) and disordered ZnO models: displacement of the Zn atom is (b) 0.005 Å, (c) 0.1 Å and (d) 0.2 Å in the *z*-direction.

This journal is © The Royal Society of Chemistry 2014

J. Mater. Chem. C, 2014, **2**, 10164–10174 | **10169**

ZnO per unit cell. The ratio of $c/a = 1.588$ deviates slightly from the ideal value of $c/a = \sqrt{8/3} = 1.633$.[45,80] The calculations suggest that the chemical nature of the bonding in the hexagonal wurtzite phase of neutral clusters is more covalent, *i.e.* this tetrahedral coordination is characteristic for covalent bonding between sp³-hybridized atoms and our results are in good agreement with previous theoretical[81–84] and experimental data.[22,23]

Fig. 5 shows that the band structures for ordered and disordered ZnO models are characterized by well-defined direct electronic transitions. For ordered and disordered ZnO models, the top of the valence band (VB) is located at Γ point. The band gap is 3.11, 3.06, 3.01 and 2.86 eV for ordered and disordered models with Zn atom displacement in the *z*-direction, respectively. These electronic levels are confirmed by UV measurements (see Fig. 1(b)), and the calculated band gap for ordered ZnO model ([ZnO₄] tetragonal clusters) is in accordance with the optically measured gap found in other studies.[22,23]

Fig. 6 shows electronic diagrams, which illustrate the projected DOS ordered ZnO and disordered ZnO models. New levels are formed above the valence band (VB) in disordered models and are associated with the specific structural disorder of ZnO. This strong dispersion in (Zn–O) bonds can modify interatomic distances in the network of the material and thus promotes the emergence of different coordination environments in ZnO clusters. This result was by our group in previous studies on intermediate- and short-range defects in ZnO single crystals.[22] This behavior can be considered as an alternative argument to explain the experimental PL spectra, as it occurs in ref. 52 and 54 in which band-gap levels are assigned to oxygen defects.

An analysis of the projected DOS indicates that the VB consists mainly of O-2p orbital levels, with minor contributions of the Zn-3p and Zn-3d orbital levels. The main contribution of the conduction band (CB) is due to Zn-4s orbital levels, with a minor contribution from the O-2p orbital levels. The presence of 3d states in the VB in the four models reveals a strong bonding character between O and Zn. The same behavior is observed for the CB. First-principles quantum mechanical calculations have shown that the break in lattice symmetry due to structural disorder is responsible for electronic states in the band gap and reveals that this structure disorder promotes local polarization and a charge gradient in the structure.[20,25,26]

More recently, the cluster-to-cluster charge-transfer process in a crystal containing more than one kind of cluster was characterized by excitations involving electronic transitions between clusters.[19,20] The vacancy remaining from the electron in an otherwise ideal cluster is a "hole polaron" which has all
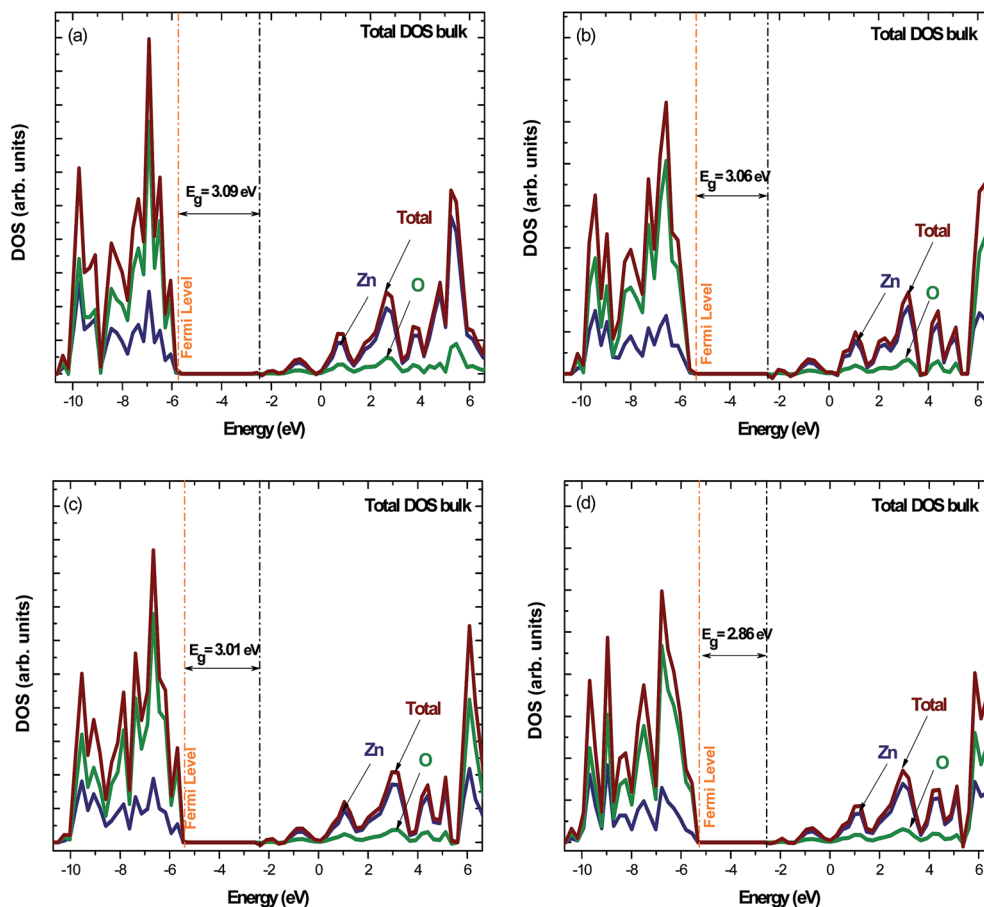

Fig. 6 Projected total density of states for the ordered (a) and disordered ZnO models: displacement of the Zn atom is (b) 0.005 Å, (c) 0.1 Å and (d) 0.2 Å in the *z*-direction.
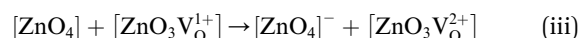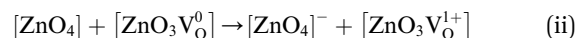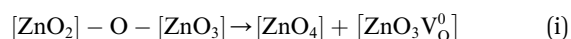
the attributes of an electron polaron, except that it is positively charged.[84] In this way, as a consequence, there is a Coulomb attraction between the electron polaron and the hole polaron and suggests that the recombination process in the crystal takes place through the medium of density defects or intermediary energy levels,[85–89] as evidenced by the UV-vis measurements.

Basically, the combination occurs between all pairs of excitons generated in the ZnO nanocrystals, resulting from different organization levels in the clusters, and is a bound state whose excitation energy lies below the conduction band threshold. We offer a possible explanation for these types of phenomena based on undercoordinated $[ZnO_4]$ clusters such as $[ZnO_3 \cdot V_O^z]$ which are associated with oxygen vacancies, since each type of hole polaron is related to the distortion $[ZnO_4]$ cluster distortion as follows (see Fig. 5, 6 and 7): (i) at low-density positive charges, there is a correspondence with the initial formation of the hole polaron (h^0) which is associated with the neutral oxygen vacancies (V_O^0), (ii) when the average positive charge density increases, the formation of hole polarons (h^+) and singly ionized oxygen vacancies (V_O^{1+}) occurs, and (iii) a large increase in charge densities is closely associated with the formation of two hole polarons ($2h^+$) due to a doubly ionized oxygen vacancy (V_O^{2+}). A graphical representation is given in Fig. 7 by using polyhedra to identify the ZnO_x ($x = 3$ and 4) cluster as building blocks. Therefore, disorder generates imbalanced charges in the structure and the formation of electrons and holes in the lattice (see Fig. 7). This fact plays a crucial role in better understanding the PL behavior.

Based on our results, we have described the wurtzite ZnO material as a framework composed of linked $[ZnO_3]$–O–$[ZnO_3]$ moieties, in which the $[ZnO_4]$ can be used to analyze its local structure. With the increase in the connection distance between a cluster $[ZnO_4]$ interacting with another cluster $[ZnO_3]$, these results show an increase in the density of negative charges in the first cluster and an increase in density of positive charges in the second cluster may be interpreted as the beginning of the formation of excitons in this system. So, we can easily show a transfer of charges involving a disordered cluster to an ordered cluster that contribute to the rationalization of chemical bond based on our quantum calculations from a model involving a cluster-to-cluster charge-transfer mechanism.

Oxygen vacancies in a disordered structure with $[ZnO_4]^-/ZnO_3V_O^z$ complex clusters are hole trapping centers according to the following equations (see Fig. 7):

$$[ZnO_2] - O - [ZnO_3] \rightarrow [ZnO_4] + [ZnO_3V_O^0] \tag{i}$$

$$[ZnO_4] + [ZnO_3V_O^0] \rightarrow [ZnO_4]^- + [ZnO_3V_O^{1+}] \tag{ii}$$

$$[ZnO_4] + [ZnO_3V_O^{1+}] \rightarrow [ZnO_4]^- + [ZnO_3V_O^{2+}] \tag{iii}$$

Structural and electronic reconstructions of all possible combinations of clusters belonging to a specific crystal are essential for an understanding of the PL phenomenon.[19,20] As the system evolves to a higher structural order, there is a decrease in structural defect densities which causes the transformation of a V_O^{2+} to V_O^{1+} and subsequently the V_O^0 oxygen vacancy in clusters. A charge redistribution process may produce an electron–hole recombination of localized excitons. Furthermore, a strong Coulomb coupling between charge
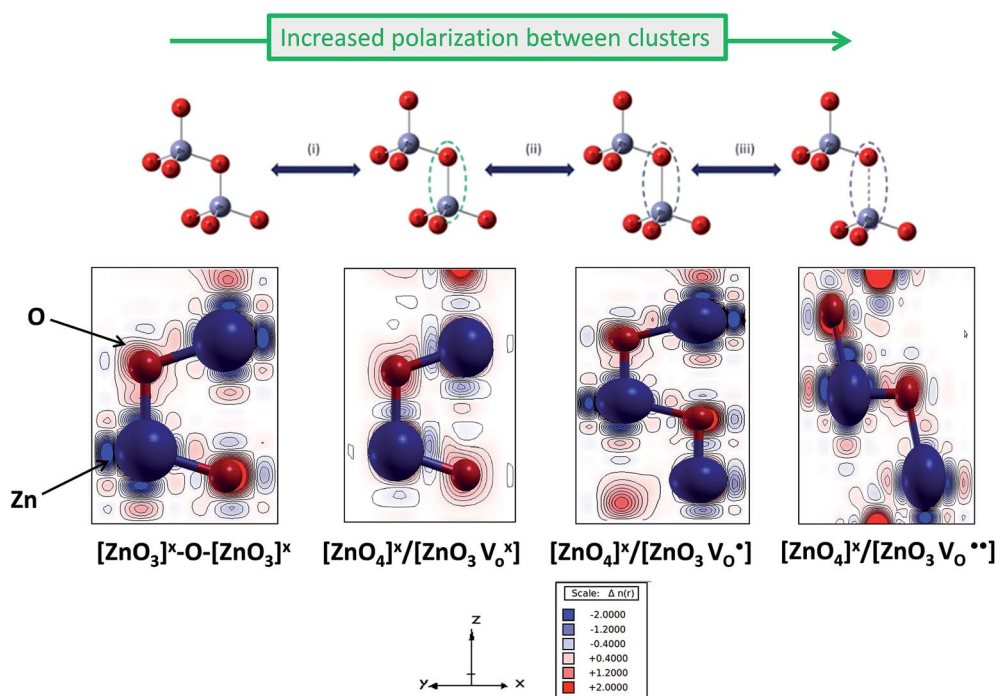

Fig. 7 Polyhedral representation to identify $[ZnO_4]^\times$, $[ZnO_4]'$, $[ZnO_3 \cdot V_O^\times]$, $[ZnO_3 \cdot VO^\cdot]$, and $[ZnO_3 \cdot VO^{\cdot\cdot}]$ clusters associated with different oxygen vacancies and holes and electron density maps for the ZnO models.

carriers promotes extremely efficient photogeneration of excitons in nanocrystals. We believe that the different types of excitons can generate different types of quantum confinements in ZnO nanocrystals and can be observed by PL measurements.

Structural and electronic order–disorder effects in semiconductor materials cause a polarization between clusters that facilitates the population of excited electronic states. In particular, the theoretical model used here is based on crystals in their ground state (lowest energy), so a model of excited states will be useful in future to clarify electronic transitions in crystalline systems as previously described by Gracia et al. for different metal oxides.[87,88] At the lowest temperature, most of the population is in the lowest energy, so this mechanism is of minimal importance for PL intensity changes in this regime, while elevating the temperature facilitates the increase in the relative populations of these excited states in ZnO and thus significantly increases the overall radiative rate.[89,90]

4. Conclusions

To summarize, from the quantitative analysis of the results obtained from a combination of experimental and theoretical approaches, we have shown a correlation between structural and electronic order–disorder effects that triggers both EPR measurements and PL properties at different temperatures in ZnO nanocrystals obtained by the MAH method. XRD, UV-vis, FE-SEM, EDXS, EPR, PL measurements and theoretical calculations were extensively employed to investigate the structural and optical properties of the wurtzite ZnO nanocrystal synthesized by the MAH method. Furthermore, we developed the cluster-to-cluster charge-transfer process mechanism to associate the structural and electronic deformations of the $[ZnO_4]$ constituent clusters of this material. It appears that the concept of ideal $[ZnO_4]$ and distorted $[ZnO_3V_O^z]$ clusters (where $V_O^z = V_O^0$, V_O^{1+} and/or V_O^{2+}) is capable of accounting for the EPR measurements and PL emissions quite satisfactorily. Our model can also be applied to other systems besides ZnO. These results have shown that the symmetry breaking process in the structure of these nanocrystals, associated with order–disorder local effects, is responsible for electronic states above the conduction gap and reveals that this disordered structure promotes local polarization and a charge gradient in the structure of ZnO nanocrystals, which are crucial factors in determining the physical properties of ZnO. Controlling order–disorder effects mean designing the properties as a function of applications and enlarge our perspective on the different complex interactions in the nanoworld. We believe that these results will help us to better understand the origin and the mechanism involved in this PL process and still more accurate theoretical calculations and experimental data in order to confirm this hypothesis are now in progress.

Acknowledgements

Notes and references

1 A. Janotti and C. G. Van de Walle, Rep. Prog. Phys., 2009, 72, 126501.

2 T. Dietl, Nat. Mater., 2010, 9, 965.

3 P. Yang, H. Yan, S. Mao, R. Russo, J. Johnson, R. Saykally, N. Morris, J. Pham, R. He and H.-J. Choi, Adv. Funct. Mater., 2002, 12, 323.

4 W. Gehlhoff and A. Hoffmann, Appl. Phys. Lett., 2012, 101, 262106.

5 B. Kulyk, Z. Essaidi, V. Kapustianyk, B. Turko, V. Rudyk, M. Partyka, M. Addou and B. Sahraoui, Opt. Commun., 2008, 281, 6107.

6 B. Kulyk, Z. Essaidi, J. Luc, Z. Sofiani, G. Boudebs, B. Sahraoui, V. Kapustianyk and B. Turko, J. Appl. Phys., 2007, 102, 113113(1–6).

7 K. Okazaki, T. Shimogaki, K. Fusazaki, M. Higashihata, D. Nakamura, N. Koshizaki and T. Okada, Appl. Phys. Lett., 2012, 101, 211105.

8 V. Ischenko, S. Polarz, D. Grote, V. Stavarache, K. Fink and M. Driess, Adv. Funct. Mater., 2005, 105, 1945.

9 P. G. Baranov, S. B. Orlinskii, C. de Mello Donega and J. Schmidt, Appl. Magn. Reson., 2010, 39, 151.

10 H. Kaftelen, K. Ocakoglu, R. Thomann, S. Tu, S. Weber and E. Erdem, Phys. Rev. B: Condens. Matter Mater. Phys., 2012, 86(014113), 1.

11 M. Stefan, S. V. Nistor and D. Ghica, Cryst. Growth Des., 2013, 13, 1350.

12 V. Kapustianyk, B. Turko, A. Kostruba, Z. Sofiani, B. Derkowska, S. Dados-Seignon, B. Barwinski, Y. Eliyashevskyi and B. Sahraoui, Opt. Commun., 2007, 269, 346.

13 H. P. He, Y. J. Wang, J. R. Wang and Z. Z. Ye, Phys. Chem. Chem. Phys., 2013, 15, 7484.

14 O. Pascu, E. Carenza, M. Gich, S. Estrade, F. Peiro, G. Herranz and A. Roig, J. Phys. Chem. C, 2012, 116, 15108.

15 T. N. Glasnov and C. O. Kappe, Chem.–Eur. J., 2011, 17, 11956.

16 I. Bilecka and M. Niederberger, Nanoscale, 2010, 2, 1358.

17 M. Baghbanzadeh, L. Carbone, P. D. Cozzoli and C. O. Kappe, Angew. Chem., Int. Ed., 2011, 50, 11312.

18 M. Baghbanzadeh, S. D. Skapin, Z. C. Orel and C. O. Kappe, Chem.–Eur. J., 2012, 18, 5724.

19 F. A. La Porta, M. M. Ferrer, Y. V. B. Santana, C. W. Raubach, V. M. Longo, J. R. Sambrano, E. Longo, J. Andrés, M. S. Li and J. A. Varela, J. Alloys Compd., 2013, 555, 153.

20 V. M. Longo, L. S. Cavalcante, E. C. Paris, J. C. Sczancoski, P. S. Pizani, M. S. Li, J. Andrés, E. Longo and J. A. Varela, J. Phys. Chem. C, 2011, 115, 5207.

21 D. P. Volanti, M. O. Orlandi, J. Andrés and E. Longo, *CrystEngComm*, 2011, **12**, 1696.

22 R. C. Lima, L. R. Macario, J. W. M. Espinosa, V. M. Longo, R. Erlo, N. L. Marana, J. R. Sambrano, M. L. dos Santos, A. P. Moura, P. S. Pizani, J. Andrés, E. Longo and J. A. Varela, *J. Phys. Chem. A*, 2008, **112**, 8970.

23 A. P. de Moura, R. C. Lima, M. L. Moreira, D. P. Volanti, J. W. M. Espinosa, M. O. Orlandi, P. S. Pizani, J. A. Varela and E. Longo, *Solid State Ionics*, 2010, **181**, 775.

24 C. Burda, X. Chen, R. Naryan and M. A. El-Sayed, *Chem. Rev.*, 2005, **105**, 1025.

25 Y. V. B. de Santana, C. W. Raubach, M. M. Ferrer, F. A. La Porta, J. R. Sambrano, V. M. Longo, E. R. Leite and E. Longo, *J. Appl. Phys.*, 2011, **110**, 123507.

26 L. S. Cavalcante, V. M. Longo, A. A. Batista, J. A. Varela, M. O. Orlandi, E. Longo and M. S. Li, *CrystEngComm*, 2012, **14**, 853.

27 J. M. Ziman, *Models of Disorder. The Theoretical Physics of Homogeneously Disordered Systems*, Cambridge University Press, Cambridge, 1979, p. 525.

28 J. A. Weil and J. R. Bolton, *Electron Paramagnetic Resonance: Elementary Theory and Practical Applications*, John Wiley & Sons, Inc., New Jersey, 2nd edn, 2007.

29 F. Viñes, A. Iglesias-Juez, F. Illas and M. Fernández-García, *J. Phys. Chem. C*, 2014, **118**, 1492.

30 A. D. Becke, *J. Chem. Phys.*, 1993, **98**, 5648.

31 C. Lee, W. Yang and R. G. Parr, *Phys. Rev. B: Condens. Matter Mater. Phys.*, 1988, **37**, 785.

32 R. Dovesi, V. R. Saunders, C. Roetti, R. Orlando, C. M. Zicovich-Wilson, F. Pascale, B. Civalleri, K. Doll, N. M. Harrison, I. J. Bush, P. D. Arco and M. Llunell *CRYSTAL09 Users Manual*, University of Torino, 2009.

33 M. F. Peintinger, D. V. Oliveira and T. Bredow, *J. Comput. Chem.*, 2013, **34**, 451.

34 H. J. Monkhorst and J. D. Pack, *Phys. Rev.*, 1976, **13**, 5188.

35 A. R. Albuquerque, M. L. Garzim, I. M. G. dos Santos, V. M. Longo, E. Longo and J. R. Sambrano, *J. Phys. Chem. A*, 2012, **116**, 11731.

36 A. R. Albuquerque, J. Maul, E. Longo, I. M. G. dos Santos and J. R. Sambrano, *J. Phys. Chem. C*, 2013, **117**, 7050.

37 A. L. J. Pereira, L. Gracia, A. Beltrán, P. N. Lisboa-Filho, J. H. D. da Silva and J. Andrés, *J. Phys. Chem. C*, 2012, **116**, 8753.

38 A. Kokalj, *J. Mol. Graphics Modell.*, 1999, **17**, 176.

39 L. S. Cavalcante, J. C. Sczancoski, V. M. Longo, F. S. de Vicente, J. R. Sambrano, A. T. de Figueiredo, C. J. Dalmaschio, M. S. Li, J. A. Varela and E. Longo, *Opt. Comm.*, 2008, **281**, 3715.

40 F. A. La Porta, J. Andrés, M. S. Li, J. R. Sambrano, J. A. Varela and E. Longo, *Phys. Chem. Chem. Phys.*, 2014, **16**, 20127.

41 T. A. Mulinari, F. A. La Porta, J. Andrés, M. Cilense, J. A. Varela and E. Longo, *CrystEngComm*, 2013, **15**, 7443.

42 M. Jianzhong, J. Liu, Y. Bao, Z. Zhu and H. Liu, *Cryst. Res. Technol.*, 2013, **48**, 251.

43 B. L. Caetano, C. V. Santilli, F. Meneau, V. Briois and S. H. Pulcinelli, *J. Phys. Chem. C*, 2011, **115**, 4404.

44 C. R. A. Catlow, S. T. Bromley, S. Hamad, M. Mora-Fonz, A. A. Skol and S. M. Woodley, *Phys. Chem. Chem. Phys.*, 2010, **12**, 786.

45 B. Ludi and M. Nieberger, *Dalton Trans.*, 2013, **42**, 12554.

46 J. M. Spaeth and H. Overhof, *Point Defects in Semiconductors and Insulators*, Springer, Berlin, 2003, p. 490.

47 H. Kaftelen, K. Ocakoglu, R. Thomann, S. Tu, S. Weber and E. Erdem, *Phys. Rev. B: Condens. Matter Mater. Phys.*, 2012, **86**, 014113.

48 C. Drouilly, J. M. Krafft, F. Averseng, S. Casale, D. Bazer-Bachi, C. Chizallet, V. Lecocq, H. Vezin, H. Lauron-Pernot and G. Costentin, *J. Phys. Chem. C*, 2012, **116**, 21297.

49 S. K. S. Parashar, B. S. Murty, S. Repp, S. Weber and E. Erdem, *J. Appl. Phys.*, 2012, **111**, 113712.

50 K. Vanheusden, C. H. Seager, W. L. Warren, D. R. Tallant and J. A. Voigt, *Appl. Phys. Lett.*, 1996, **68**, 403.

51 F. A. Salim, M. H. Weber, D. Solodovnikov and K. G. Lynn, *Phys. Rev. Lett.*, 2007, **99**, 085502.

52 R. M. Sheetz, I. Ponomareva, E. Richter, A. N. Adriotis and M. Menon, *Phys. Rev. B: Condens. Matter Mater. Phys.*, 2009, **80**, 195314.

53 S. J. Clark, J. Robertson, S. Lany and A. Zunger, *Phys. Rev. B: Condens. Matter Mater. Phys.*, 2010, **81**, 115311.

54 F. Oba, A. Togo, I. Tanaka, J. Paier and G. Kresse, *Phys. Rev. B: Condens. Matter Mater. Phys.*, 2008, **77**, 245202.

55 A. Alkauskas, J. L. Lyons, D. Steiauf and C. G. Van de Walle, *Phys. Rev. Lett.*, 2012, **109**, 267401.

56 M. Hunger and J. Weitkamp, *Angew. Chem., Int. Ed.*, 2001, **40**, 2954.

57 X. D. Chen, C. C. Ling, S. Fung, C. D. Beling, Y. F. Mei, R. K. Y. Fu, G. G. Siu and P. K. Chu, *Appl. Phys. Lett.*, 2006, **88**, 132104.

58 O. Mondal and M. Pal, *J. Mater. Chem.*, 2011, **21**, 18354.

59 Y. Zhang, J. Xu, Q. Xiang, H. Li, Q. Pan and P. Xu, *J. Phys. Chem. C*, 2009, **113**, 3430.

60 M. Willander, O. Nur, J. R. Sadaf, M. I. Qadir, S. Zaman, A. Zainelabdin, N. Bano and I. Hussain, *Materials*, 2010, **3**, 2643.

61 M. Willander, M. Q. Israr, J. R. Sadaf and O. Nur, *Nanophotonics*, 2012, **1**, 99.

62 I. Hussain, N. Bano, S. Hussain, Y. Soomro, O. Nur and M. Willander, *Materials*, 2011, **4**, 1260.

63 I. Hussain, N. Bano, S. Hussain, O. Nur and M. Willander, *J. Mater. Sci.*, 2011, **46**, 7437.

64 B. Kulyk, B. Sahraoui, V. Figà, B. Turko, V. Rudyk and V. Kapustianyk, *J. Alloys Compd.*, 2009, **481**, 819.

65 B. Kulyk, Z. Essaidi, V. Kapustianyk, B. Turko, V. Rudyk, M. Partyka, M. Addou and B. Sahraoui, *Opt. Commun.*, 2008, **281**, 6107.

66 Z. Sofiani, B. Sahraoui, M. Addou, R. Adhiri, M. A. Lamrani, L. Dghoughi, N. Fellahi, B. Derkowska and W. Bala, *J. Appl. Phys.*, 2007, **101**, 063104.

67 L. Wang and N. C. Giles, *J. Appl. Phys.*, 2003, **94**, 973.

68 D. J. Gargas, H. Gao, H. Wang and P. Yang, *Nano Lett.*, 2011, **11**, 3792.

69 L. K. Van Vugt, S. Rühle, P. Ravindran, H. C. Gerritsen, L. Kuipers and D. Vanmaekelbergh, *Phys. Rev. Lett.*, 2006, **97**, 147401.

70 J. Chen, L. Aé, C. Aichele and M. C. Lux-Steiner, *Appl. Phys. Lett.*, 2008, **92**, 161906.

71 Y. Yamada, H. Yasuda, T. Tayagaki and Y. Kanemitsu, *Phys. Rev. Lett.*, 2009, **102**, 247401.

72 C. Bauer, G. Boschloo, E. Mukhtar and A. Hagfeldt, *Chem. Phys. Lett.*, 2004, **387**, 176.

73 E. Longo, E. Orhan, F. M. Pontes, C. D. Pinheiro, E. R. Leite, J. A. Varela, P. S. Pizani, T. M. Boschi, F. Lanciotti Jr, A. Beltran and J. Andres, *Phys. Rev. B: Condens. Matter Mater. Phys.*, 2004, **69**, 125115.

74 M. L. Moreira, J. Andrés, E. Longo and J. A. Varela, *Cryst. Growth Des.*, 2008, **9**, 833.

75 E. Orhan, F. M. Pontes, C. D. Pinheiro, T. M. Boschi, E. R. Leite, P. S. Pizani, A. Beltran, J. Andres, J. A. Varela and E. Longo, *J. Solid State Chem.*, 2004, **177**(11), 3879.

76 J. C. Sczancoski, M. D. R. Bomio, L. S. Cavalcante, M. R. Joya, P. S. Pizani, J. A. Varela, E. Longo, M. S. Li and J. Andrés, *J. Phys. Chem. C*, 2009, **113**(14), 5812.

77 P. Dev, H. Zeng and P. Zhang, *Phys. Rev. B: Condens. Matter Mater. Phys.*, 2010, **82**, 165319.

78 E. Nielsen and R. N. Bhatt, *Phys. Rev. Lett.*, 2007, **76**, 161202(R).

79 H. Y. Playford, L. R. Owen, I. Levin and M. G. Trucker, *Annu. Rev. Mater. Res.*, 2014, **44**, 13.1.

80 C. Klingshirn, *ChemPhysChem*, 2007, **8**, 782.

81 D. Gryaznov, E. Blokhin, A. Sorokine, E. A. Kotomin, R. A. Evarestov, A. Bussmann-Holder and J. Maier, *J. Phys. Chem. C*, 2013, **117**(27), 13776.

82 N. L. Marana, V. M. Longo, E. Longo, J. B. L. Martins and J. R. Sambrano, *J. Phys. Chem. A*, 2008, **112**, 8956.

83 N. L. Marana, J. R. Sambrano and A. R. de Souza, *Quim. Nova*, 2010, **33**, 810.

84 W. Barford, *J. Phys. Chem. A*, 2013, **117**, 2665.

85 W. Shockley and W. T. Reed Jr, *Phys. Rev.*, 1952, **87**, 835.

86 M. Ansari-Rad, J. A. Anta and J. Bisquert, *J. Phys. Chem. C*, 2013, **117**, 16275.

87 L. Garcia, V. M. Longo, L. S. Cavalcante, A. Beltrán, W. Avansi, M. S. Li, V. R. Mastelaro, J. A. Varela, E. Longo and J. Andrés, *J. Appl. Phys.*, 2011, **110**, 043501.

88 L. Garcia, J. Andrés, V. M. Longo, J. A. Varela and E. Longo, *Chem. Phys. Lett.*, 2010, **493**, 141.

89 L. S. Cavalcante, M. A. P. Almeida, W. Avansi Jr, R. L. Tranquilin, E. Longo, N. C. Batista, V. R. Mastelaro and M. S. Li, *Inorg. Chem.*, 2012, **51**, 10675.

90 X. Cai, J. E. Martin, L. E. Shea-Rohwer, K. Gong and D. F. Kelley, *J. Phys. Chem. C*, 2013, **117**, 7902.